



Prochelators triggered by hydrogen peroxide provide hexadentate iron coordination to impede oxidative stress

Marina G.D. Leed^a, Natalie Wolkow^b, David M. Pham^a, Catherine L. Daniel^a,
Joshua L. Dunaief^b, Katherine J. Franz^{a,*}

^a Department of Chemistry, Duke University, Durham, NC 27708-0346, United States

^b F. M. Kirby Center for Molecular Ophthalmology, Scheie Eye Institute, University of Pennsylvania, Philadelphia, PA 19104, United States

ARTICLE INFO

Article history:

Received 17 March 2011

Received in revised form 27 May 2011

Accepted 31 May 2011

Available online xxx

Keywords:

Oxidative stress

Reactive oxygen species

Fenton chemistry

Chelation therapy

Iron

Copper

ABSTRACT

Prochelators are agents that have little affinity for metal ions until they undergo a chemical conversion. Three new aryl boronate prochelators are presented that are responsive to hydrogen peroxide to provide hexadentate ligands for chelating metal ions. TRENBSIM (tris[(2-(4,4,5,5-tetramethyl-1,3,2-dioxaborolan-2-yl)benzylidene)-2-aminoethyl]amine), TRENBSAM (tris[(2-(4,4,5,5-tetramethyl-1,3,2-dioxaborolan-2-yl)benzoyl)-2-aminoethyl]amine), and TB (tris[(2-boronic acid-benzyl)2-aminoethyl]amine) convert to TRENBSIM (tris[salicylideneamino]ethyl]amine), TRENBSAM (tris[(2-hydroxybenzoyl)-2-aminoethyl]amine), and TS (tris[2-hydroxybenzyl]2-aminoethyl]amine), respectively. The prochelators were characterized by ¹¹B NMR, and the structures of TRENBSAM, TRENBSIM, and the Fe(III) complex of TS were determined by X-ray crystallography. Of the three prochelator/chelator pairs, TB/TS was identified as the most promising for biological applications, as they prevent iron and copper-induced hydroxyl radical generation in an in vitro assay. TB has negligible interactions with metal ions, whereas TS has apparent binding constants (log *K'*) at pH 7.4 of 15.87 for Cu(II), 9.67 Zn(II) and 14.42 for Fe(III). Up to 1 mM TB was nontoxic to retinal pigment epithelial cells, whereas 10 μM TS induced cell death. TS protected cells against H₂O₂-induced death, but only within a 1–10 μM range. TB, on the other hand, had a much broader window of protection, suggesting that it may be a useful agent for preventing metal-promoted oxidative damage.

© 2011 Elsevier Inc. All rights reserved.

1. Introduction

Iron and copper are transition elements that are essential cofactors for a number of proteins and enzymes that are critical to human life. Their beneficial roles, however, are counterbalanced by their potential contribution to cellular oxidative stress via Fenton chemistry (Eqs. 1a and 1b), wherein Fe(II) (or Cu(I)) is oxidized by hydrogen peroxide to produce the very damaging hydroxyl radical, a reactive oxygen species (ROS) that causes lipid peroxidation, DNA damage and eventual cell death [1]. Eqs. (1a) and (1b) become catalytic in metal if cellular reductants like ascorbic acid, glutathione, or superoxide recycle the Fe(III) or Cu(II) to Fe(II) or Cu(I). The presence of such redox-active iron or copper that is not well regulated by the normal cellular homeostatic mechanisms has been implicated in a growing list of diseases, including macular degeneration, Alzheimer's and Parkinson's disease [2–8]. Chelating these metal ions in non-redox-active forms is emerging as a potential therapeutic intervention to minimize metal-mediated oxidative stress [9–11].



Iron chelation therapy has been used for decades for the treatment of iron overload diseases [12]. In these applications, the goal is to reduce the level of non-transferrin bound iron in the plasma. The most widely used treatment consists of high doses of the membrane impermeable chelator desferrioxamine B (DFO), which has a short in vivo half-life and is poorly absorbed, requiring patients to endure long subcutaneous transfusions 5–7 days a week [12]. The high dosage required for treatment can lead to deterioration in vision, cardiac health and overall growth [13,14]. It has been speculated that some of the side effects of chelation therapy may be the result of off-target metal binding by the administered drug that leads to deficiency in other essential metals [15]. While one DFO molecule provides sufficient donor atoms to fill the six coordination sites of iron and form stable non-reactive complexes, it can also bind other metal ions. In order to prevent off-target metal sequestration, it would be ideal to have a chelating agent that maintains a hexadentate coordination environment like DFO but also has the ability to commandeer redox-active metal ions that are causing cellular damage without adversely affecting healthy metal status.

* Corresponding author. Tel.: +1 919 660 1541; fax: +1 919 660 1605.

E-mail address: katherine.franz@duke.edu (K.J. Franz).

In our lab we have developed a series of prochelators that are unmasked to their active chelating forms in response to hydrogen peroxide [16–20]. Utilizing hydrogen peroxide as a prochelator trigger in principle exposes chelators exclusively to errant metal ions in the Fenton cycle in order to prevent the buildup of dangerously high concentrations of hydroxyl radicals. Previous prochelators are built on either tridentate or bidentate scaffolds, requiring two or three molecules to completely bind one Cu(II) or Fe(III) ion. Partially coordinated iron can still interact with ROS and may promote the rate of hydroxyl radical production, rather than retard it [21]. Thus it would be ideal to design responsive iron chelators that can fully encapsulate iron under physiological conditions.

Here we introduce a new series of prochelators, depicted in Fig. 1, designed to minimize iron and copper induced oxidative stress. These prochelators are masked with pinacol boronic esters or boronic acids, which are oxidized to phenols by hydrogen peroxide, revealing hexadentate metal chelators. Related tripodal hexadentate chelators have been well studied as models of siderophores, [22] the naturally occurring small molecules produced by several microorganisms to acquire iron from their environment. The hexadentate scaffold is advantageous because it provides all six binding sites to fully coordinate a metal ion as an octahedral complex, thus lowering the risk of open coordination sites that allow access to inner-sphere reactivity at the metal center.

2. Experimental

2.1. Materials and instrumentation

All chemicals and solvents were obtained from Sigma-Aldrich or Acros Organics and used as received, unless otherwise noted. Triethylamine was vacuum distilled and stored under Ar over dried molecular sieves before use. Dioxane was dried with a Pure Solv MD Solvent Purification System by Innovative Technology and used immediately. TREN SAM (tris[(2-hydroxybenzoyl)-2-aminoethyl]amine) [22] and TREN SIM (tris[(salicylideneamino)ethyl]amine) [23,24] were prepared by following reported procedures. NMR data were collected on either a Varian Inova 400 MHz or 500 MHz spectrometer with chemical shifts reported in ppm and *J* values in Hz. The splitting of proton resonances in the reported ¹H NMR spectra is defined as s = singlet, d = doublet, t = triplet and m = multiplet. The ¹¹B NMR spectra were referenced to an external standard of boron trifluoride diethyl etherate (0.0 ppm) in CDCl₃. UV/visible (UV/Vis) spectra were recorded on a Cary 50 UV/Vis spectrophotometer with a 1-cm quartz cuvette. Fluorescence spectra were recorded on a Jobin-Yvon–Horiba Fluorolog 3 fluorimeter in a 1-cm pathlength quartz cell. Excitation and emission slit widths were 5 nm and excitation spectra

were collected from 300 to 450 nm with emission held at 510 nm. Electrospray ionization (ESI) mass spectra were recorded on an electrospray quadrupole ion trap mass spectrometer (1100 Series LC/MSD Trap, Agilent, Palo Alto, CA); high resolution mass spectra (HRMS) were recorded on a time of flight mass spectrometer (Agilent 6224 TOF). IR spectra were collected on a Nicolet 360 FT-IR. Elemental analysis was performed by Columbia Analytical Services, Tucson, AZ.

2.2. Synthesis

Bsalate (methyl 2-(4,4,5,5-tetramethyl-1,3,2-dioxaborolan-2-yl)benzoate). A portion of 1-*n*-butyl-3-methylimidazolium tetrafluoroborate (3 mL) was heated in vacuo with stirring at 80 °C for 30 min before the addition of methyl-2-iodobenzoate (1.5 mmol, 0.23 mL) and palladium acetate (0.045 mmol, 0.030 g). This mixture was heated to 100 °C while stirring under Ar for 90 min to yield a brownish green solution. A portion of triethylamine (4.5 mmol, 0.68 mL) was added at room temperature. The reaction was returned to heat before adding pinacolborane (3 mmol, 0.44 mL). A subtle shift to a greener color was observed with the evolution of bubbles. After 1 h, the solution had become clear light green and was allowed to react overnight. The reaction was then cooled to r.t. and extracted into diethyl ether. The organic portion was washed with dilute HCl (0.1 M) and dried over MgSO₄. The product was purified as a yellow oil by silica gel column chromatography (9:1 hexanes:ethyl acetate, *R_f* = 0.25) in 34% yield. ¹H NMR (500 MHz, CDCl₃) 7.90 (d, *J* = 8.0, 1 H), 7.81 (d, *J* = 8.0, 1 H), 7.38 (d, *J* = 4.0, 1 H), 7.29 (t, *J* = 7.0, 1 H), 3.77 (s, 3 H), 1.29 (s, 12 H). ¹¹B NMR (160 MHz, CDCl₃) ppm 31.632 (s). MS (*m/z*): 263.14 (Calc. 263.14) (*M* + *H*⁺, 100%). IR (cm⁻¹): 2980 (C–H), 1730 (C=O), 1150 (C–O ester), 1110 (C–O, ether).

TRENBSAM (Tris[(2-(4,4,5,5-tetramethyl-1,3,2-dioxaborolan-2-yl)benzoyl)-2-aminoethyl]amine). A portion of Bsalate (3 mmol, 0.786 g) was added dropwise to a solution of tris(2-ethylamino)amine (1 mmol, 0.146 g) in 2 mL anhydrous methanol. The solution was refluxed at 100 °C under Ar for 30 min in a sealed round-bottom flask. The solution was cooled to r.t. and the solvent removed by evaporation to produce a yellow oil. The product was purified as a light yellow solid in 65% yield by silica gel column chromatography (7:3 hexanes:ethyl acetate, 0–10% MeOH, *R_f* = 0.103). ¹H (500 MHz, CDCl₃): 7.89 (d, *J* = 8.0, 3 H), 7.79 (d, *J* = 8.0, 3 H), 7.36 (m, 3 H), 7.27 (m, 3 H), 3.74 (s, 12 H), 1.27 (s, 36H). ¹¹B (160 MHz, CDCl₃): 33.69 and 24.16 ppm. HRMS (*m/z*): 837.4873 (Calc. 837.4874) (*M* + *H*⁺, 100%). IR (cm⁻¹): 2966 (C–H), 1645 (C=O), 1455 (N–H), 1110 (C–O). UV/Vis (PBS pH 7.4): λ_{max}(ε) = 287 nm (5565 M⁻¹ cm⁻¹).

TRENBSIM (Tris[(2-(4,4,5,5-tetramethyl-1,3,2-dioxaborolan-2-yl)benzylidene)-2-aminoethyl]amine). A portion of 2-formylphenylboronic acid, pinacol ester (3 mmol, 0.66 mL) was added to a solution of tris(2-

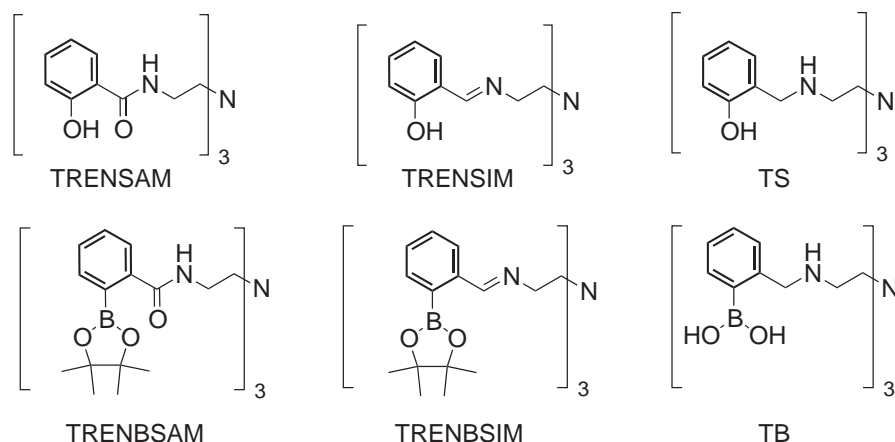


Fig. 1. Hexadentate chelators (top) and prochelators (bottom).

ethylamino)amine (1 mmol, 0.146 g) in 2 mL anhydrous methanol. The solution was stirred with heating to 60 °C for 3 h. The solvent was removed by rotary evaporation and the product used without further purification. ^1H NMR (500 MHz, CDCl_3): 8.35 (s, 3 H), 7.57 (d, $J=7.0$, 3 H), 7.42 (t, $J=7.0$, 3 H), 6.85 (t, $J=7.5$, 3 H), 5.24 (d, $J=7.4$, 3 H), 3.98 (t, $J=4.5$, 6 H), 2.99 (s, 6 H), 1.30 (s, 36 H). ^{11}B NMR (160 MHz, CDCl_3): 14.80. HRMS (m/z) 789.5028 (Calc. 789.5027) ($\text{M} + \text{H}^+$, 100%).

TRENBASIM (Tris[(2-(boronic acid)benzylidene)-2-aminoethyl]amine). A portion of 2-formylphenylboronic acid (3.1 mmol, 0.480 g) was added to a solution of tris(2-ethylamino)amine (1 mmol, 0.149 mL) in 3 mL anhydrous methanol. The solution was stirred with heating to 60 °C. After 2 h, the clear yellow liquid condensed to a yellow solid. A sample was removed for characterization and the product used without further purification. ^1H NMR (500 MHz, CD_3OD): 8.35 (s, 3 H), 7.56 (s, 3 H), 7.51 (t, 3 H), 7.12 (s, 3 H), 6.00 (s, 3 H), 3.75 (s, 6 H), 2.94 (s, 6 H). ^{11}B NMR (160 MHz, CDCl_3): 14.80. MS (m/z): 560.2 (Calc. 560.27) ($\text{M} + \text{OH}^-$, 70%).

TB (Tris[(2-boronic acid-benzyl)2-aminoethyl]amine). A portion of TRENBASIM (1 mmol, 0.548 g) was taken into a minimal amount of methanol and cooled to 0 °C over an ice bath before stirring with the addition of NaBH_4 (15 mmol, 0.57 g). After the evolution of H_2 gas was complete, the solution was warmed to r.t. and stirred an additional 30 min. The reaction was quenched with 10 mL H_2O and extracted with 5×50 mL diethyl ether. The aqueous layer was subjected to continuous extraction with 300 mL of diethyl ether overnight. The organic portions were combined and evaporated to dryness to afford a white solid in 40% yield. Purity was confirmed by reverse phase HPLC, with a single peak at 18.5 min on a X-Bridge C18 column in a linear 41-min gradient from 7 to 93% acetonitrile in water. ^1H NMR (400 MHz, CD_3OD): 7.46 (s, 3 H), 7.20 (s, 9 H), 4.10 (s, 6 H), 3.08 (s, 6 H), 2.98 (s, 6 H). ^{13}C (101 MHz, CDCl_3): 184.64, 131.57, 128.35, 127.64, 124.00, 79.89, 55.39, 51.48, 46.05. ^{11}B NMR (160 MHz, D_2O): 9.64. IR (cm^{-1}): 3350 (N–H), 2960 (C–H), 1110 (C–O). HRMS (m/z): 531.3140 (Calc. 531.3043) ($\text{M} - \text{H}_2\text{O}^+$, 100%). UV/Vis (PBS pH 7.4): $\lambda_{\text{max}}(\epsilon) = 270$ nm ($1546 \text{ M}^{-1} \text{ cm}^{-1}$).

TS (Tris[2-hydroxybenzyl)2-aminoethyl]amine). In a procedure slightly modified from what has been previously reported, [24] TRENBSIM (1 mmol, 0.458 g) was dissolved in 10 mL methanol and cooled to 0 °C. To this was added NaBH_4 (4 mmol, 0.1513 g) and the reaction was stirred until the evolution of H_2 gas was complete, approximately 2 h. The solution was warmed to r.t. and stirred an additional 30 min. The solvent was removed by rotary evaporation, the remaining material taken into diethyl ether and washed with 3×10 mL water. Evaporation of the solvent produced a yellow solid in 98% yield. ^1H NMR (400 MHz, CDCl_3): 7.14 (t, $J=7.7$, 3 H), 6.97 (d, $J=7.2$, 3 H), 6.76 (t, $J=8.6$, 6 H), 3.99 (s, 6 H), 2.73 (t, $J=5.5$, 6 H), 2.59 (t, $J=5.4$, 6 H). ^{13}C (101 MHz, CDCl_3): 158.04, 128.82, 128.60, 122.01, 119.01, 116.39, 54.04, 52.17, 45.86. IR (cm^{-1}): 3250 (O–H), 2832 (C–H), 1588 (N–H). MS (m/z): 465.2 (Calc. 465.28) ($\text{M} + \text{H}^+$, 100%). UV/Vis (PBS pH 7.4): $\lambda_{\text{max}}(\epsilon) = 276$ nm ($5920 \text{ M}^{-1} \text{ cm}^{-1}$).

[FeHTS]OTf. Iron (II) triflate (0.269 g, 0.76 mmol) was added to a solution of TS (0.353 g, 0.76 mmol) in 3 mL anhydrous acetonitrile to produce a purple solution. This solution was refluxed for 10 min before cooling to r.t. over an hour. The solid was washed with cold diethyl ether to give a deep purple, microcrystalline powder in 69% yield. UV/Vis (PBS pH 7.4): $\lambda_{\text{max}}(\epsilon) = 483$ nm ($4440 \text{ M}^{-1} \text{ cm}^{-1}$). HRMS (m/z): 518.1974 (Calc. 518.1980 for $[\text{FeHTS}]^+$, 100%). Elem. Anal. Found: C, 49.34; H, 5.10; N, 8.26. Calc. for $\text{C}_{28}\text{H}_{34}\text{F}_3\text{FeN}_4\text{O}_6\text{S}$: C, 50.38; H, 5.13; N, 8.39. Although the elemental analysis, especially for C, was somewhat unsatisfactory, the mass spectral data reasonably support the formula.

2.3. Crystallization, X-ray data collection and structure solution refinement

Purified solutions of TRENBSAM failed to yield crystalline material; however, a methanolic solution of unpurified material produced cocrystals of TRENBSAM with an equivalent of methyl-2-iodobenzoate.

The slow evaporation of a wet chloroform solution of TRENBSIM produced crystals suitable for X-ray diffraction which contained a water in the crystal lattice.

Attempts to grow crystals of [FeHTS]OTf suitable for X-ray diffraction were unsuccessful. As an alternative, [FeHTS] ClO_4 was prepared in small quantity by combining equimolar portions of TS and $[\text{Fe}(\text{bipyridine})_3](\text{ClO}_4)_2$ in boiling acetonitrile and stirring for several h [** Caution! Perchlorate salts of transition metals complexes are potentially explosive and should be handled with care. Although no explosions were encountered in this study, metal perchlorates could detonate upon heating]. Upon cooling, cold ether was added to precipitate residual $[\text{Fe}(\text{bipyridine})_3](\text{ClO}_4)_2$ and slow evaporation of the filtrate yielded deep red prismatic crystals of [FeHTS] ClO_4 . The asymmetric unit contains two Fe complexes along with one molecule of acetonitrile.

Data for TRENBSAM, TRENBSIM and [FeHTS] ClO_4 were collected at 298, 273 and 296 K, respectively, on a Bruker Kappa Apex II CCD diffractometer equipped with a graphite monochromator and a Mo K α fine focus sealed tube ($\lambda = 0.71073 \text{ \AA}$) operated at 1.75 kW power (50 kV, 35 mA). The detector was placed at a distance of 5.0 cm from the crystal. A total of 2655 frames were collected with a scan width of 0.5° and an exposure time of 30.0 s/frame. The frames were integrated with the Bruker SAINT v7.12A software package using a narrow-frame integration algorithm. Empirical absorption corrections were applied using SADABS v2.10 and the structures were checked for higher symmetry with PLATON v1.07. The structures were solved by direct methods with refinement by full-matrix least-squares based on F^2 using the Bruker SHELXTL Software Package. All non-hydrogen atoms were refined anisotropically. Hydrogen atoms of sp^2 hybridized carbons and nitrogens were located directly from the difference Fourier maps; all others were calculated. A table of crystal data and structure refinement for all three structures can be found in Table S1 of the Supplementary Information, which also contains full X-ray crystallographic data in CIF format.

2.4. ^{11}B NMR pH titration

Samples containing 20 mM TB and 25 mM HEPES were prepared in D_2O and the pH was adjusted by addition of 2 M NaOH or 2 M HClO_4 . The reported pH values are corrected by +0.4 pH units to the pH meter reading of the deuterated samples, per convention [25].

2.5. Kinetics of prochelator oxidation

The rate of oxidation of prochelator to chelator was determined under pseudo-first order conditions of excess H_2O_2 . TRENBSAM and TB were dissolved in DMSO and phosphate buffered saline (PBS), respectively, and diluted to 100 μM in PBS buffer, pH 7.4, with less than 1% DMSO in TRENBSAM solutions. Spectra were taken every 12 s immediately after the addition of 3–50 mM H_2O_2 ; data were collected for 15 min or until no further spectral changes were detected. The changes in absorbance at 276 nm for TB and 277 nm for TRENBSAM were used to follow the reaction. The negative slope of the linear fit of $\ln[(A - A_f)/(A_0 - A_f)]$ vs time in s gives the observed rate constant k_{obs} (where A_0 and A_f are the absorbance of the intact prochelator and the final chelator product, respectively). The slope of the line through the plot of k_{obs} vs $[\text{H}_2\text{O}_2]$ provides the second-order rate constant, k ($\text{M}^{-1} \text{ s}^{-1}$). This value k can then be used to determine the rate of oxidation as defined in Eq. (2).

$$\text{Rate} = k[\text{H}_2\text{O}_2][\text{prochelator}] \quad (2)$$

2.6. Deoxyribose assay

Deoxyribose assays were conducted on a Perkin Elmer Victor 1420 plate reader. The formation of hydroxyl radicals was measured by

using a 2-deoxyribose oxidative degradation assay [26,27]. The assay was conducted in a 96-well plate, which allowed large numbers of repetitions with high precision. Solutions of H₂O₂ and ascorbic acid were made fresh daily, while other solutions were made weekly. In a typical experiment, the following reagents were added sequentially to 50 mM NaH₂PO₄ (to make 100 μL) with final concentrations listed in parentheses: chelator or prochelator (0–400 μM), FeCl₃ or Cu(ClO₄)₂ (10 μM), 2-deoxyribose (15 mM), H₂O₂ (400 μM), and ascorbic acid (2 mM). The plate was heated to 37 °C with shaking for 1 h before quenching with 100 μL TBA (thiobarbituric acid, 57.1 μM) and 100 μL TCA (trichloroacetic acid, 23.1 μM) and heating at 100 °C for 20 min. The high temperature was achieved by suspending the plate with wire above a hot water bath at 100 °C. After cooling to room temperature and removing the lid, the absorbance at 490 nm was measured. To ensure accurate values, the absorbance of a blank well of buffer alone was subtracted from each well. The data were reported as the ratio A/A₀, where A is the absorbance at 490 nm of each well, and A₀ is the absorbance at 490 nm of the reaction mixture without the added chelator or prochelator. All experiments were performed in at least quadruplicate, with error bars reflecting any standard deviation within the runs.

2.7. Electrochemistry

Electrochemistry experiments were conducted with a Cypress System 2R cyclic voltammeter, model BASi-CGME. Solutions of 1 mM ligand were prepared in 3 mL of nitrogen-degassed HEPES buffer (10 mM HEPES, 100 mM NaCl) at pH 6.0, 7.4, or 8.2. The auxiliary and reference electrodes were a platinum wire and a silver reference electrode (Ag/AgCl in 3.5 M KCl). A hanging mercury drop was used as the working electrode. Three drops of mercury were expelled before collecting data. Cyclic voltammetry experiments were performed at various sweep rates (50–500 mV/s), starting at both high and low potentials to determine the reversibility of the reactions. Corrected potentials are reported relative to the normal hydrogen electrode (NHE) in water and were estimated using the equation $E_{\text{NHE(aq)}} = E_{\text{Ag/AgCl(aq)}} + 0.205 \text{ V}$ [28].

2.8. Determination of apparent binding affinity of TS for Cu(II) and Fe(III)

Apparent binding constants (*K'*) of TS for Cu(II) and Fe(III) were determined spectrophotometrically from competition experiments with EDTA in PBS buffer at pH 7.4. The experiment establishes an exchange equilibrium (*K*_{ex}) between EDTA and TS for binding Cu(II) or Fe(III), as shown in Eq. (3) in which 'M' is defined as either Fe(III) or Cu(II). The equilibrium expression *K*_{ex} (Eq. (4)) comprises the individual equilibrium expressions for each ligand, defined in Eqs. (5) and (6). The values for *K'*_{CuEDTA} (15.81) and *K'*_{FeEDTA} (15.93) were calculated from the overall binding constants 18.7 and 25.0 respectively, adjusted for pH [29].



$$K_{\text{ex}} = \frac{[\text{EDTA}] \times [\text{MTS}]}{[\text{TS}] \times [\text{MEDTA}]} = \frac{K'_{\text{MTS}}}{K'_{\text{MEDTA}}} \quad (4)$$



Solutions of EDTA (0.08 mM), Cu(ClO₄)₂ or Fe(ClO₄)₃ (0.05 mM) and TS (0–0.8 mM) were combined in 2 mL pH 7.4 PBS buffer (10 mM NaH₂PO₄, 154 mM NaCl) and allowed to equilibrate for at least 24 h. The excess of chelator-to-metal ensured that the metal ions remained

coordinated at all times to prevent hydrolysis. After equilibration (as determined by the stabilization of the UV/Vis spectra), the absorbance at 414 nm due to the [CuTS] complex (or 483 nm for the [FeTS] complex) was recorded and converted to a concentration based on the respective extinction coefficient ([CuTS] $\epsilon_{414} = 1095 \text{ M}^{-1} \text{ cm}^{-1}$ and [FeTS] $\epsilon_{483} = 4444 \text{ M}^{-1} \text{ cm}^{-1}$). Values for [EDTA], [TS] and [CuEDTA] were then determined from mass balance equations and a *K*_{ex} was calculated for each sample. Sixteen separate samples were prepared with varying concentrations of TS. The average *K*_{ex} value was then used to determine *K'*_{CuTS} = 15.87 and *K'*_{FeTS} = 14.42.

2.9. Determination of apparent binding affinity of TS for Zn(II)

The apparent affinity of TS for Zn(II) at pH 7.4 was determined spectrophotometrically by a competition reaction between TS and PAR (4-(2-pyridylazo)resorcinol) in a method similar to that previously reported [30]. The exchange reaction and its equilibrium expression are shown in Eqs. (7) and (8), while the individual equilibria are shown in Eqs. (9) and (10), where *K'* refers to the apparent binding constant under these conditions of buffer and pH. A solution of 100 μM PAR in 1 mL HEPES (10 mM HEPES, 100 mM NaCl, pH 7.4) was used as a background spectrum for the titration. To this solution was added 5 μM ZnSO₄ (2 μL of a 2.5 mM stock solution) and the absorbance spectrum from 200 to 800 nm was collected. To this solution were added 2 μM aliquots of TS (2 μL of a 1 mM solution) and the decrease in the absorbance at 500 nm was monitored until no further spectral changes were detected.



$$K_{\text{ex}} = \frac{[\text{PAR}]^2 \times [\text{ZnTS}]}{[\text{TS}] \times [\text{ZnPAR}_2]} = \frac{K'_{\text{ZnTS}}}{K'_{\text{ZnPAR}_2}} \quad (8)$$



The concentration of [ZnPAR₂] is obtained at each titration point from its extinction coefficient ($\epsilon = 66000 \text{ M}^{-1} \text{ cm}^{-1}$) and the concentrations of the other components in Eq. (8) are calculated from mass balance equations. With *K*_{ex} in hand, and the known affinity of PAR (log *K'* = 12.34) for zinc, [30] the apparent zinc binding constant (*K'*_{ZnTS}) of TS is calculated according to Eq. (8). Three separate trials were averaged to give an overall value.

2.10. Assessment of relative binding affinity of TS for calcium

A stock solution of the fluorescent calcium indicator fura-4F (Invitrogen) was made by dissolving 500 μg indicator in 500 μL ice-cold HEPES buffer, pH 7.4. Calcium chloride stocks were made to 10 mM with HEPES buffer (10 mM HEPES, 100 mM NaCl). To a fluorescence cuvette containing 2 mL HEPES buffer was added 1 μM indicator and 1 μM calcium. This spectrum set the baseline for the completely complexed indicator. To this sample were added aliquots of TS (to a total 1.5 mM) to evaluate the relative binding affinity of TS for calcium.

2.11. Cell viability assays

The spontaneously immortalized human retinal pigment epithelial cell line ARPE-19 was purchased from American Type Culture Collection (ATCC, Manassas, VA). Cells were kept at 37 °C, 5% CO₂, in a humidified incubator, and were grown in DMEM-F12 media, which is a 1:1 mixture of DMEM (Invitrogen) and F-12 (Invitrogen), with

10% heat-inactivated Fetal Bovine serum (Hyclone), 1% of 100× Penicillin/Streptomycin (Invitrogen) and 1% of 100× L-glutamine (Invitrogen, 25030). For experiments, passage 24–32 cells were used. Cells were plated into 24-well plates, where they were allowed to grow until confluence (approximately 4 days). The lactate dehydrogenase (LDH) release assay for cell death was obtained from Roche Diagnostics and performed on a Perkin Elmer Victor³ 1420 plate reader.

A peroxide kill curve was established to determine a working toxic dose of hydrogen peroxide. Confluent cells were washed 3 times with warm phenol-free MEM media (Invitrogen), and treated with 1 mL of MEM or 0 μM–5 mM H₂O₂ in MEM. Cells were incubated at 37 °C for 15 h. After 15 h, an LDH assay was performed to measure cell death. Briefly, a 150-μL aliquot of the supernatant was collected from each well and centrifuged at 1000 rpm for 5 min to precipitate any cellular debris. Then, 25 μL of supernatant was aliquoted into 3 separate wells on a 96-well plate for each sample. 75 μL of calcium- and magnesium-free DPBS (Invitrogen) was added to each well, and a separate sample acted as a background control. 100 μL LDH reagent was then added to each well before incubation in the dark at room temperature for 30 min. The absorbance at 490 nm was measured. Concentrations of 200 μM peroxide were used as the lethal peroxide dose for subsequent experiments.

For TS and TB experiments, each 24-well plate had triplicate repeats of each treatment. Each plate had a low control (MEM alone) and high control (200 μM peroxide). All experiments were repeated on at least two separate occasions. For toxicity experiments, TS was dissolved in DMSO to make a 10 mM TS solution. This was further diluted to make 10 nM–50 μM TS in 1% DMSO, in warm MEM. TB solutions in MEM were prepared immediately prior to use by sonication for ~10–20 min in a 35 °C water bath. The 1 mM TB solution was filter-sterilized and then diluted to make the appropriate concentrations. Cells were washed 3 times with warm MEM, before addition of 1 mL of TS or TB of the appropriate concentration to each well of cells. As low controls, 3 wells on each plate were treated with MEM alone and 3 wells with MEM + 1% DMSO; as the high control, 3 wells on each plate were treated with 200 μM peroxide to cause complete cell death. Cells were returned to 37 °C incubator for 15 h, after which an LDH assay was performed, as described above.

To test TS and TB protection against lethal doses of H₂O₂, fresh TB and TS stocks were prepared as described above and diluted in MEM to the appropriate final concentration. Cells were washed 3 times with MEM, and the TS/TB dilutions were added to cells along with 200 μM final concentration of hydrogen peroxide. The LDH assay was performed 15 h after treatment.

To analyze LDH assay results, the absorbance values at 490 nm were used to calculate % cell viability as follows:

$$\% \text{ Cytotoxicity} = \frac{[(\text{experimental value} - \text{low control}) / (\text{high control} - \text{low control})] \times 100}{100}$$

$$\% \text{ Viability} = 100 - \% \text{ Cytotoxicity}$$

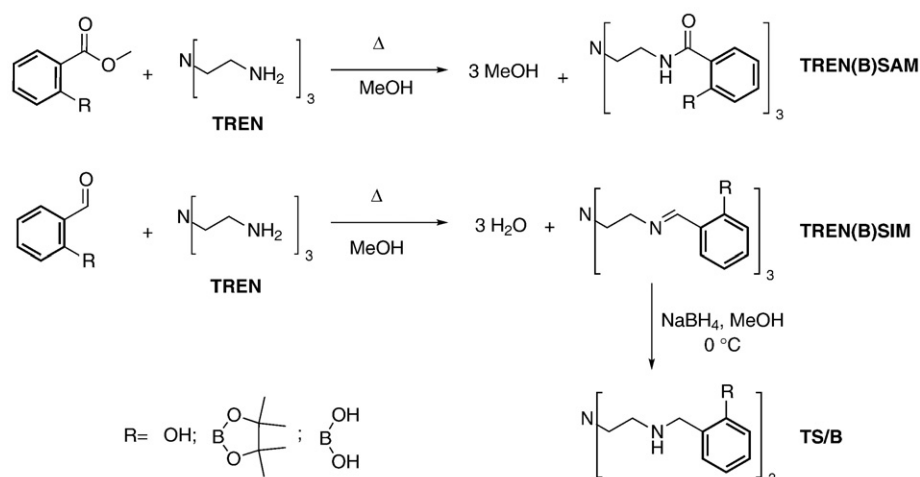
3. Results

3.1. Synthesis

In order to expand on the existing families of bi- and tri-dentate prochelators, [16–20] hexadentate metal prochelator and chelator pairs were designed. To have an appropriate binding pocket to accommodate metal ions, three phenol moieties were suspended from the central nitrogen atom of the compound tren, (tris(2-ethylamino)amine) such that the linkage provided additional donor atoms for potential hexadentate chelation. Three such prochelator/chelator pairs have been synthesized. All three chelators provide an O₃N₃ donor set for metal complexation, where the three oxygens are phenolates in all cases, but the three nitrogen donors vary from amide to imine to amine. The apical nitrogen on the tren backbone provides an additional potential coordination site. The synthesis and structures of these compounds are shown in Scheme 1.

For consistency in nomenclature we have adopted a system in line with that used by the Raymond lab, which first characterized the hexadentate chelator TRENSAM [22]. A condensation of tren with a salicylate yields the amide containing products TRENBSAM or TRENBSAM, depending on whether the substituents on the aryl ring are boronates (B) or phenols. When the aryl compound is changed from a salicylate to a salicylaldehyde, the imine containing products TRENBSIM and TRENBSIM are obtained. Reduction of the imine by sodium borohydride provides the amine-containing compounds, which we name simply TB or TS. The prochelator TB was also prepared as the pinacol ester, TBpin; however, the material isolated after aqueous workup and HPLC purification contained a mixture of boronic acid and boronic ester units, indicating that some of the pinacol esters were hydrolyzed during the isolation procedure. Since TBpin (wherein all three borons are coordinated by pinacol ester units) was never obtained in pure form, the pure boronic acid compound TB was used for subsequent studies.

TRENBSIM and TRENBSIM, with imine linkages between the backbone and the iron-binding motif, are not stable to hydrolysis



Scheme 1. Synthesis of hexadentate chelators TRENBSAM, TRENBSIM and TS (R=OH) and prochelators TRENBSAM, TRENBSIM and TB (R=boronic ester or boronic acid).

and rapidly decompose to the corresponding amine and aldehyde in either buffer or water. Thus, this pair of compounds was not as fully characterized and was not included in further studies. In contrast, the compounds utilizing amide or amine linkages (TRENBSAM/TRENBSAM and TB/TS, respectively) are stable in buffer, making them better targets for the physiological chelation of iron.

The synthesis and purification of prochelators TRENBSAM and TRENBSIM and the chelators TRENBSAM, TRENBSIM and TS proceed unremarkably. The isolation of TB from reaction side products requires more diligent treatment due to its inherent water solubility. This solubility is likely due to a solvent molecule coordinating to the boron atom, as has also been seen by others [31–33] [34]. Extraction into the organic phase from water thus proceeds slowly.

3.2. Structures of prochelators

The crystal structures of two prochelators were solved. TRENBSAM crystallized from methanol, while TRENBSIM crystallized from chloroform. Both structures, shown in Fig. 2, show a clearly defined tripod configuration in which the bulky pinacol methyl groups are forced to the outside of the tripod. The apical nitrogen is not protonated in either structure. The boron atom in both cases is tetravalent, three donors come from the aryl carbon and two pinacol oxygens, while the fourth coordination site is provided by the amide oxygen, in the case of TRENBSAM, or the imine nitrogen, in TRENBSIM. The average bond length of the pinacol O–B bonds in both TRENBSIM and TRENBSAM is 1.433(3) Å. The length of the fourth bond is dependent on the donor, as the N–B bond lengths in TRENBSIM range from 1.688(3) to 1.713(3) Å, while the lengths of the O–B bonds from the amide oxygens in TRENBSAM are slightly shorter, from 1.641(4) to 1.683(4) Å.

Because only two of the three prochelators are crystalline in nature, we rely on ^{11}B NMR to provide structural information for all three prochelators. The ^{11}B NMR spectra of all three prochelators (see

Supplementary information) were collected and compared to determine the boron environment in each compound.

In general, three-coordinate R–B–(OR)₂ species have chemical shifts of 20–40 ppm, while four-coordinate species have shifts between 0 and 20 ppm [35,36]. These generalities are complicated by the fact that solvents with donating character can interact with boron and thus shift the spectra to fall in the range of four coordinate species when in solution [37]. The chemical shift characteristic of a dative N–B bond falls near 14 ppm in a wide variety of solvents, while the insertion of a solvent molecule between boron and a nearby amine results in peaks found at 8–10 ppm [31,33,37–40].

The ^{11}B NMR spectrum of TRENBSAM shows a very distinct shift of 33.70 ppm in CDCl₃, with a minor peak at 24.16 ppm, suggesting that the boron is predominately tricoordinate in chloroform solution, with a minor tetracoordinate species. This result contrasts the tetracoordinate species that crystallized from methanol. In contrast, the chemical shift of TRENBSIM in CDCl₃ appears at 14.91 ppm, strongly suggesting that the N–B dative bond observed in the crystal structure persists in chloroform solution. Whether this configuration is retained in water cannot be tested due to the hydrolysis of the imine bond in TRENBSIM. The ^{11}B NMR spectrum of TB was obtained in D₂O at neutral pH due to poor solubility in organic solvents. The spectrum clearly shows two boron environments, though in unequal proportions. The major peak appears at 9.64 ppm likely due to solvent coordination to boron, while a minor peak attributed to boron hydroxylation is shifted upfield to 3.98 ppm.

3.3. ^{11}B NMR pH titration of TB

The effect of pH on the boron environment was determined by measuring the shift of the major peak in the ^{11}B NMR spectra of solutions containing TB over a range of pH. Scheme 2 presents the boron environments of TB possible with changing pH. The structure on the left exists at low pH, in which the secondary amine of the scaffold arm is protonated. As the pH increases, two intermediate speciations are

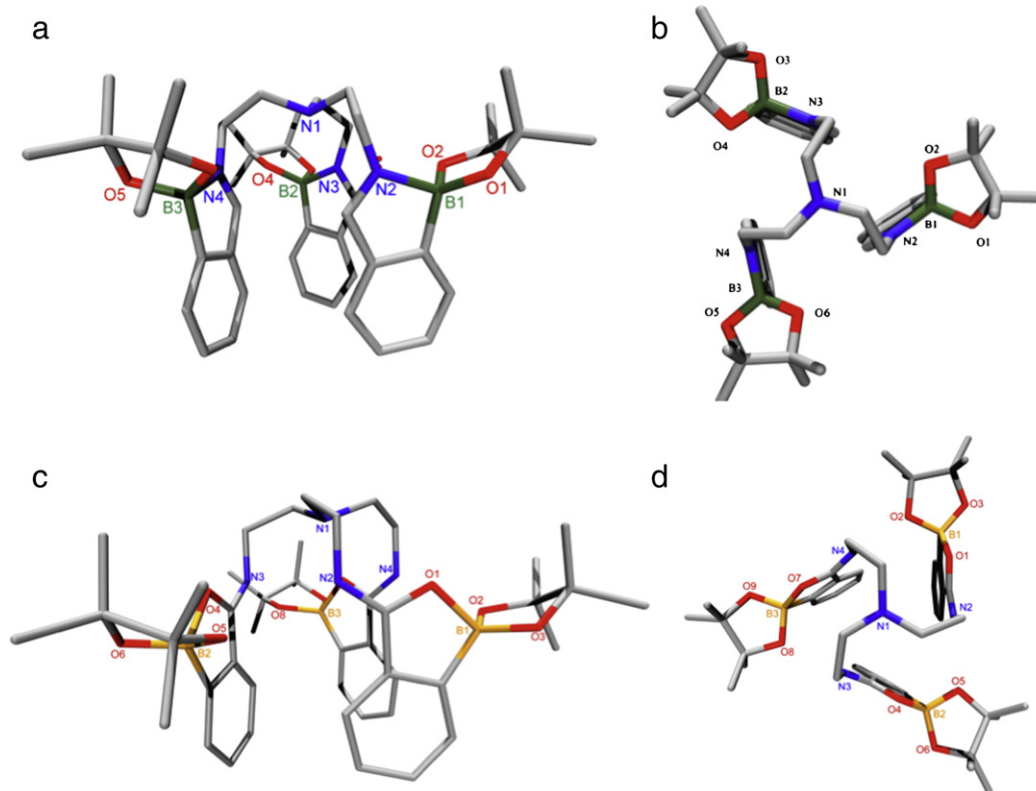
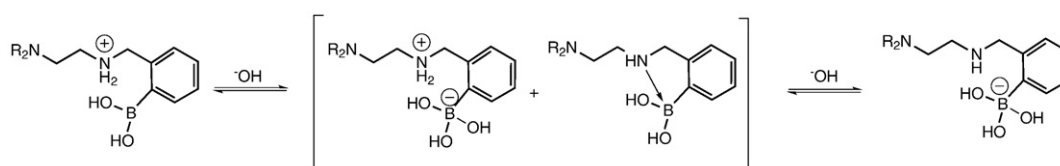


Fig. 2. Side and top views of the crystal structures of TRENBSIM (a and b, respectively) and TRENBSAM (c and d) shown as stick diagrams. Hydrogen atoms have been omitted for clarity.



Scheme 2. Boron environments of TB as a function of pH.

possible. In one scenario, a water molecule inserts between the amine and the boron, inducing a change to a tetravalent boron and formation of a zwitterion. The other scenario involves deprotonation of the amine, leaving it free to donate electron density to the boron to create a N–B dative bond, which also creates a four-coordinate environment around the boron and an overall neutral compound. At high pH, the amine becomes deprotonated and three hydroxyl groups complete the tetraivalent coordination around boron to provide an overall anionic species.

Solutions of deuterium oxide containing TB in HEPES buffer were made to 11 different pH values by the addition of 2 M HClO₄ or NaOH. The spectra of these solutions, shown in Fig. 3, give more information about the boron environment as the solution chemistry changes. The broad signal centered around -5 ppm is due to the boron present in the glass of the probe, and is unavoidable at these concentrations despite the use of quartz NMR tubes. At low pH, the boron is in a trigonal environment as indicated by the shift of 19 ppm, and the secondary amine of the scaffold arm is likely protonated. An increase in pH causes a decrease of this species, and promotes the formation of a new species with a shift of ~ 8 ppm. As depicted in Scheme 2, the intermediate species could either be one in which there is an N–B dative bond, or an inserted water molecule. While the shift indicates a boron atom with some tetracoordinate character, it is not characteristic of N–B bond formation, and we conclude that the solvated TB is present from pH 6.9 to 12.8. A third distinct boron environment emerges at pH values greater than 10. This species is attributed to the

deprotonation of the ammonium ion to give the anionic species shown at the far right in Scheme 2. This value is in line with the general range for both ammonium deprotonation (pH 9–10) and for other *ortho* amino-boronates [41]. From this titration, we conclude that TB exists as both the tricoordinate boron species and the solvent coordinated species at pH 7.4, as depicted by the two structures on the left side of Scheme 2.

3.4. Kinetics of prochelator-to-chelator conversion by H₂O₂

To determine the efficacy of TRENBSAM and TB as hydrogen peroxide responsive chelators, the rate of oxidation was studied under pseudo first-order conditions of excess hydrogen peroxide. TRENBSIM was not studied due to the immediate hydrolysis of the imine linkage in aqueous solution. Reactions were monitored spectrophotometrically in solutions of 20 mM phosphate buffered saline at pH 7.4. The time-dependent spectra in Fig. 4a show that the addition of 30 mM H₂O₂ to a 100 μ M sample of TB results in an absorbance increase at 277 nm that stops changing after 4 min. The spectra in Fig. 4b of TRENBSAM under the same conditions show a decrease in absorbance around 250 nm with an increase around 310 nm and a clean isosbestic point at 293 nm. In contrast to TB, the spectral changes of TRENBSAM only stabilize after 30 min of reaction. The final spectra in both Fig. 4a and b match those of the independently prepared chelators TS and TRENAM, respectively, indicating complete conversion of the prochelators to their chelator counterparts. Furthermore, the mass

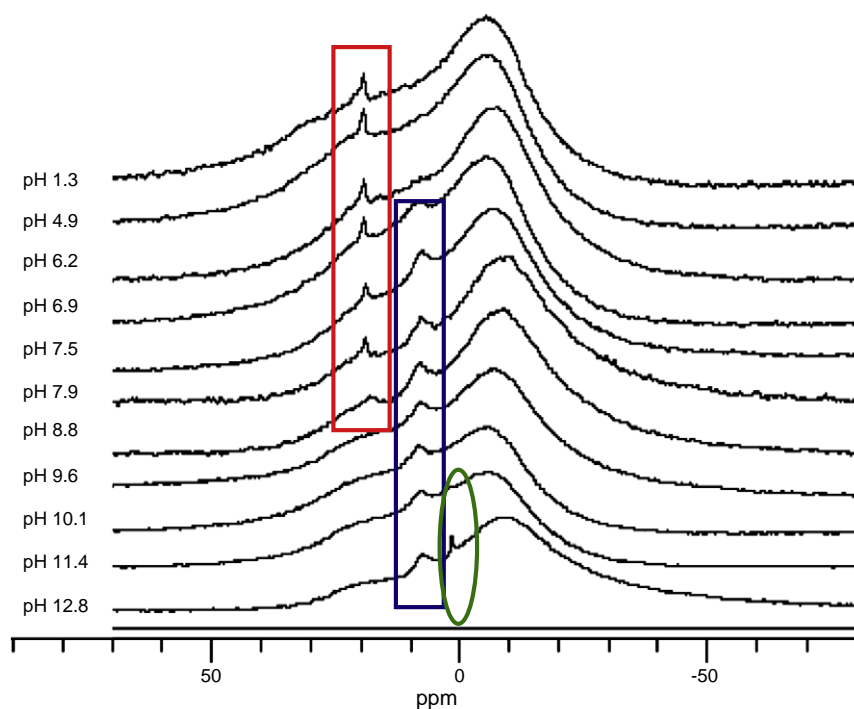


Fig. 3. ¹¹B NMR pH titration of TB. Solutions of 10 mM TB with 25 mM HEPES in D₂O were probed by ¹¹B NMR. The red box on the left highlights peaks with a shift ~ 19 ppm. Peaks in the center blue box have a shift of ~ 8 ppm, while the green circled features shift to ~ 2 ppm. The broad feature at -5 ppm is an artifact of boron in the glass of the NMR probe. (For interpretation of the references to color in this figure legend, the reader is referred to the web version of this article.)

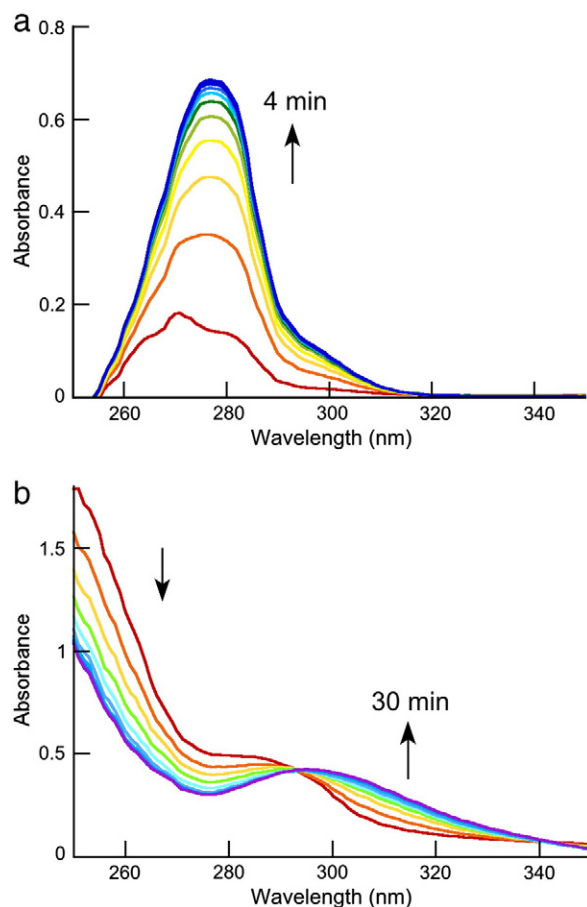


Fig. 4. UV/Vis spectra showing the reaction of 100 μM TB (a) and 100 μM TRENBSAM (b) with 30 mM hydrogen peroxide; both samples are in 20 mM PBS pH 7.4. The conversion of TB to TS is complete within 4 min, whereas TRENBSAM takes over 30 min to convert to TRENBSAM under these conditions.

of the respective chelator was detected in the oxidized samples by mass spectrometry.

As shown in Fig. 5, the observed pseudo first-order rate constant (k_{obs}) is linearly dependent on the concentration of hydrogen

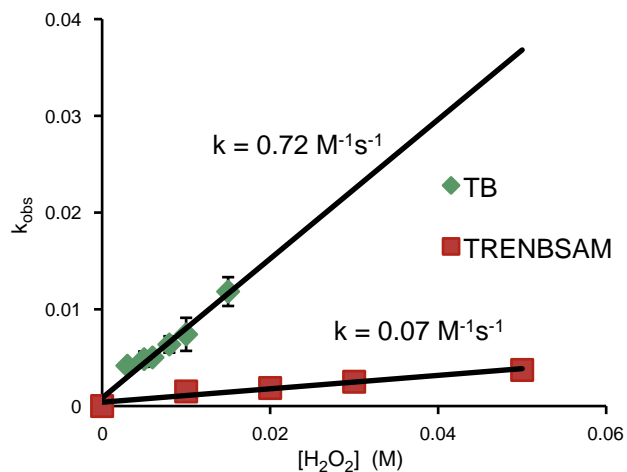


Fig. 5. Plot of observed rate constants versus hydrogen peroxide concentration for 100 μM TB (green diamonds) and 100 μM TRENBSAM (red squares) in pH 7.4 phosphate buffered saline. The initial rates of oxidation differ by a factor of 10, as determined by measurement of spectrophotometric changes at 276 nm (TRENBSAM) and 277 nm (TB). (For interpretation of the references to color in this figure legend, the reader is referred to the web version of this article.)

peroxide; the second order rate constant (k) is obtained from the slope of this line. For TB, k is $0.72 \text{ M}^{-1}\text{s}^{-1}$, whereas it is only $0.07 \text{ M}^{-1}\text{s}^{-1}$ for TRENBSAM.

3.5. Determination of apparent metal binding affinity of TS

The apparent binding affinity of TS for several biologically relevant metal ions was determined by a series of competition experiments in aqueous buffered solutions at pH 7.4. Copper and iron affinities were determined by spectrophotometric titration with the competing chelator EDTA. The absorbance of [CuTS] was measured at 414 nm, as the spectrum of [CuEDTA] has no absorbance at this wavelength. Increasing concentrations of TS added to a solution of [CuEDTA] result in an increase of the absorbance at 414 nm (Fig. S1, Supplementary information). Utilization of the equilibrium Eqs. (3)–(6) led to the calculation of an apparent binding constant $\log K' = 15.87$ at pH 7.4.

A similar competition between EDTA and TS for iron(III) (Fig. S2, Supplementary information) led to the determination of a $\log K'$ value of 14.42. It is worth noting that the formation of the [FeTS] complex was much slower than in the case of copper. In the case of the Fe competition studies, the absorbance spectra stabilized only after 24 h, indicating a kinetically slow exchange between EDTA and TS. Similarly, the direct addition of an iron(III) source like FeCl_3 to a solution of TS results in the slow generation of the colored [FeTS] complex, again indicative of a slow binding reaction. On the other hand, direct addition of iron(II) salts to aqueous or methanol solutions of TS results in the immediate formation of a colored [Fe(II)TS] species (not shown). These results suggest that TS can rapidly coordinate Fe(II) in solution, but that the compound rapidly oxidizes to the Fe(III) species in aerobic environments.

In addition to Cu(II) and Fe(III), the affinity of TS for Zn(II) was also investigated. A competition study with PAR demonstrates that TS can effectively compete for Zn(II), as seen in the decrease of the distinct ZnPAR_2 absorbance at 500 nm (Fig. S3, Supplementary information). Given the affinity of PAR for zinc ($\log K' = 12.34$) and the Eqs. (7)–(10), an apparent binding affinity of $\log K' = 9.67$ for zinc by TS was calculated.

The fluorescent calcium indicator fura-4F was used to establish a binding affinity of TS for Ca(II). A change in the fluorescence of the Ca-indicator solution was not observed until TS was added to nearly 1000 times greater concentration, establishing that TS is unable to compete for calcium in the presence of fura-4F. Because the binding affinity of fura-4F for Ca(II) is 0.77 μM , [42,43] the relative affinity of TS for calcium must be significantly weaker.

While it was anticipated that TS would bind divalent and trivalent d-block metal ions, the replacement of the phenols on TS with boronic acids was anticipated to inhibit metal binding by the prochelators. However, there are still four amines on TB that could provide a metal-binding site, particularly for copper. In order to test this possibility, the absorbance spectra of TB in the presence and absence of Cu(II) was recorded and compared with that of [CuTS]. As seen in Fig. 6, TB shows negligible interaction with copper in solution, whereas the chelator TS forms a copper complex with a distinct feature at 420 nm. A similar experiment with Fe(III) likewise indicated negligible interaction between the prochelator and iron (data not shown).

3.6. Crystal structure of an iron–TS complex

While the amine phenol ligand TS has been crystallized with several trivalent lanthanides as well as divalent metals like Cu(II), Ni(II) and Zn(II), there have been no reported crystal structures of an iron complex [24,44–46]. Here we report the crystal structure of [FeHTS]ClO₄, in which iron is coordinated by three phenolic oxygens, two secondary amines of the tripod arms and the apical nitrogen (Fig. 7). The amine that is not coordinated is protonated (N3), creating a positive charge that is balanced by an outer-sphere anion. The

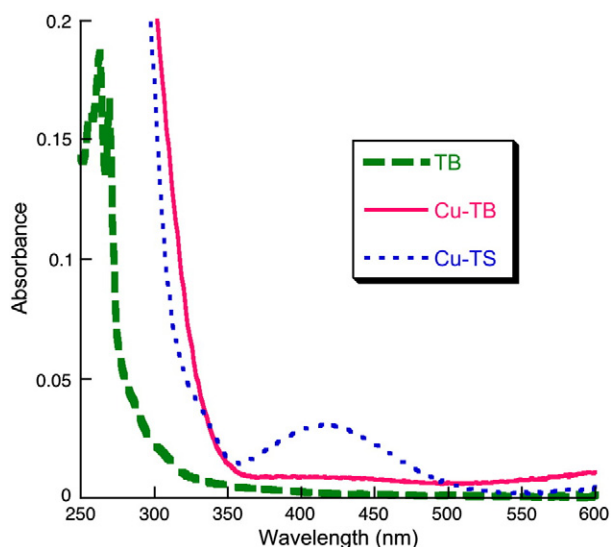


Fig. 6. UV/Vis spectra of copper binding by TS and TB. TB (green dashed line) does not bind copper (red solid line), while TS has a distinct absorbance at 420 nm (blue dotted line) upon copper binding. Conditions: 100 μ M TB, 100 μ M TS, and 100 μ M $\text{Cu}(\text{ClO}_4)_2$ in 20 mM phosphate buffer, pH 7.4. (For interpretation of the references to color in this figure legend, the reader is referred to the web version of this article.)

coordination of the apical nitrogen (N4) requires a longer bond than from the nitrogens in the arms of the ligand and causes distortion due to the formation of 5-membered rings. The average Fe–O bond lengths for $[\text{FeHTS}]\text{ClO}_4$ (1.919 Å) are consistent with those seen for iron(III) complexes.

3.7. Electrochemistry

In order to determine the redox behavior of iron coordinated by the TS ligand under physiologically relevant conditions, cyclic voltammetry experiments were conducted in pH 7.4 HEPES buffer (10 mM HEPES, 100 mM NaCl) with a mercury hanging drop electrode. No peaks were observed for solutions containing the ligand alone, but as shown in Fig. 8, the iron complex displays reversible one-electron redox behavior with a reduction potential ($E_{1/2}$, defined as the midpoint between the reduction and oxidation peaks) of

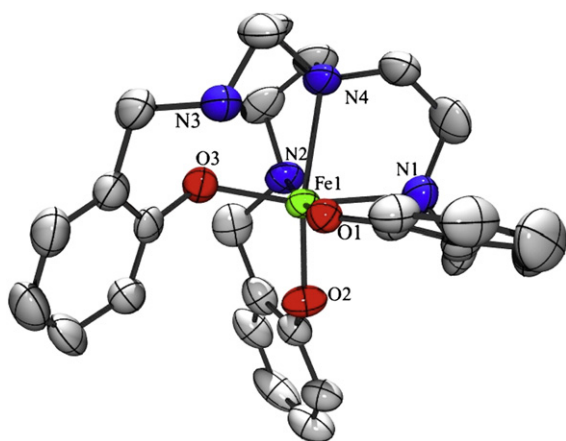


Fig. 7. Crystal structure of $[\text{FeHTS}]\text{ClO}_4$. Only one of the two Fe–TS molecules contained in the asymmetric unit is shown. Thermal ellipsoids are shown at 50% probability. Hydrogen atoms (including 2 H's on N3) and the ClO_4 anion are not shown. Selected bond distances (Å) and angles ($^\circ$): Fe–O1, 1.946(3); Fe–O2, 1.891(3); Fe–O3, 1.920(3); Fe–N1, 2.184(4); Fe–N2, 2.186(4); Fe–N4, 2.293(4); O1–Fe–O2, 99.5(1); O1–Fe–O3, 91.2(1); O2–Fe–O3, 103.6(5); O1–Fe–N1, 87.7(1); O1–Fe–N2, 172.8(1); O1–Fe–N4, 92.4(1); O2–Fe–N1, 90.6(1); O2–Fe–N2, 87.3(1); O2–Fe–N4, 162.9(1); O3–Fe–N1, 165.7(1); O3–Fe–N2, 89.1(1); O3–Fe–N4, 88.1(1); N1–Fe–N2, 90.2(1); N1–Fe–N4, 77.7(1); N2–Fe–N4, 80.4(1).

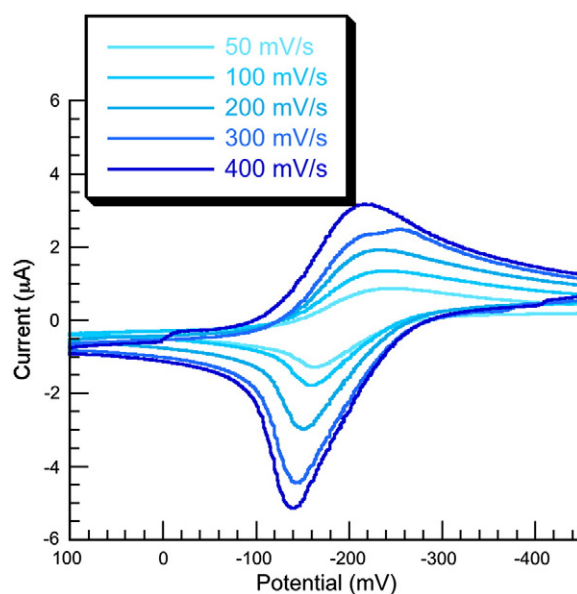


Fig. 8. Cyclic voltammograms of TS with $\text{Fe}(\text{NH}_4)_2(\text{SO}_4)_2$ (both 1 mM) in HEPES buffer at pH 7.4 at a hanging mercury drop electrode; scan rates as indicated.

–190 mV vs NHE. As expected for reversible reactions, the peaks move apart slightly and increase in magnitude as the scan rate increases. Ferrous ammonium sulfate was used in these experiments as the iron source, although similar results were obtained by using FeCl_3 (not shown). Because the reduction potential can be dependent on pH, [47] cyclic voltammetry was also conducted at pH 6.0 and 8.2. The general behavior of the complex at these pH values is consistent with that seen at pH 7.4, though the reduction potential shifts to –185 mV vs NHE at pH 6.0 and –210 mV at pH 8.2, as shown in Figs. S4 and S5 in Supplementary information.

3.8. Assessment of the inhibition of Fenton chemistry

The ability of each chelator and prochelator to prevent hydroxyl radical induced oxidative damage was determined by the deoxyribose assay. In this assay iron or copper is incubated with hydrogen peroxide and ascorbic acid to establish Fenton chemistry. The hydroxyl radicals generated by the reaction of reduced iron or copper with hydrogen peroxide attack the deoxyribose in solution, creating byproducts that can be measured colorimetrically after the addition of thiobarbituric acid. The amount of damage in the presence of chelator or prochelator is compared to that incurred in the absence of the chelator (A/A_0). Values of A/A_0 greater than one indicate increased hydroxyl radical production, while values less than one are indicative of inhibition of the Fenton reaction and therefore protection against metal-induced oxidative damage.

Both TS and TB are very protective against hydroxyl radical induced damage, as seen in Fig. 9. Even concentrations as low as 3 μ M TS or TB protect against 50% of the damage generated by either iron (Fig. 9a) or copper (9b) in the absence of chelator. However, concentrations of 200 μ M TRENBSAM or TRENBSAM offer little protection against deoxyribose damage.

3.9. Cell toxicity experiments

From analysis of the in vitro experiments described above, the prochelator/chelator combination of TB/TS emerged as the most favorable for potential biological applications. In order to determine the inherent toxicity of these compounds, ARPE-19 cells were treated with a range of concentrations of the chelator TS and prochelator TB and monitored for cell viability. Fig. 10 demonstrates that TS and TB

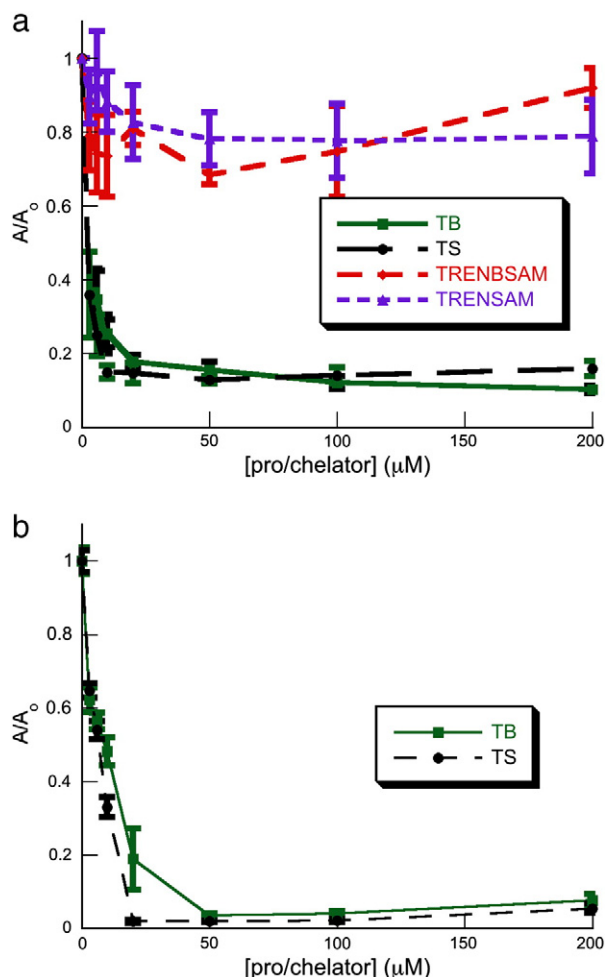


Fig. 9. Effect of hexadentate prochelators and chelators on deoxyribose degradation by (a) iron or (b) copper-induced radical formation. Conditions: $400 \mu\text{M H}_2\text{O}_2$, $10 \mu\text{M FeCl}_3$ or $10 \mu\text{M Cu}(\text{ClO}_4)_2$, 2 mM ascorbic acid, 15 mM 2-deoxyribose in pH 7.4 phosphate buffer. A and A_0 are the absorbance readings at 490 nm with and without added chelator. Values of $A/A_0 < 1$ signify protection against radical generated deoxyribose degradation.

have very different toxicity profiles. TS requires dissolution in 1% DMSO due to low aqueous solubility, although the treatment of DMSO alone does not affect cell viability. TS ($1\text{--}50 \mu\text{M}$) or TB ($1\text{--}1000 \mu\text{M}$)

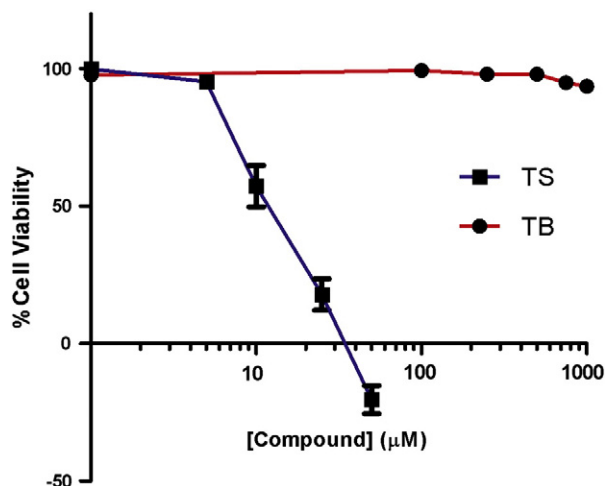


Fig. 10. Toxicity of TB and TS in ARPE-19 cells. The prochelator TB is not cytotoxic up to 1 mM , while the chelator TS induces cell death at concentrations as low as $1 \mu\text{M}$.

were applied to cells for 15 h. TS was not toxic to cells at $1 \mu\text{M}$ or $5 \mu\text{M}$, but at $10 \mu\text{M}$ it was significantly toxic, causing a 50% decrease in cell viability. TB, on the other hand, did not show cellular toxicity, even at doses as high as $1000 \mu\text{M}$.

To determine if TS and TB can protect ARPE-19 cells from lethal doses of hydrogen peroxide, cells were treated for 15 h with TS + $200 \mu\text{M}$ hydrogen peroxide, or with TB + $200 \mu\text{M}$ hydrogen peroxide. TS protected ARPE-19 cells from peroxide-induced death, but with a very narrow range of protection. TS protected approximately 40% of cells at a $0.25 \mu\text{M}$ dose and at $1\text{--}5 \mu\text{M}$ doses there was complete protection against peroxide as seen in Fig. 11. However, at doses $10 \mu\text{M}$ and higher, toxicity emerged for TS. TB also protected cells from peroxide-induced death, but had a much broader protection range than TS. TB showed a protective effect at $1 \mu\text{M}$, a higher dose than the dose at which TS started being protective. TB showed complete protection from peroxide stress at doses of $2\text{--}10 \mu\text{M}$. An increase in TB concentration to $25 \mu\text{M}$ diminished its protective effect to approximately 65–70%, where it remained all the way up to the $1000 \mu\text{M}$ dose.

4. Discussion

While the potential for using metal chelating agents to mitigate oxidative stress in a number of diseases is appealing, there are significant challenges to such a strategy to avoid unintended consequences of manipulating biological metal ions [9]. In terms of the chemistry, some of the minimum requirements include stability in aqueous solution, the ability to bind the target metal ion at physiological pH while avoiding other metal ions, and that the metal complex itself not be a catalyst for Fenton-like reactions. Because bidentate and tridentate chelators can coordinate iron in 1:1 or 1:2 complexes that actually promote Fenton chemistry instead of prevent it, [48] hexadentate chelators are desirable. Masking metal-binding groups of a chelator to create a prochelator is a strategy this lab has been exploring to prevent non-specific metal binding.

To expand on our existing tridentate and bidentate prochelators, we have introduced here a series of prochelators built on hexadentate scaffolds. Of the three prochelator/chelator pairs that were investigated, the TRENBSIM/TRENBSIM pair is the least likely to be biologically useful, as the imine linkage hydrolyzes in aqueous solution to disassemble the metal binding pocket. While the TRENAM/TRENBSAM pair is stable in water, its deficiency in terms of biological application derives from TRENAM's weak iron binding at neutral pH, [22] slow prochelator-to-chelator oxidation by hydrogen peroxide, and the lack of any inhibition against hydroxyl radical formation

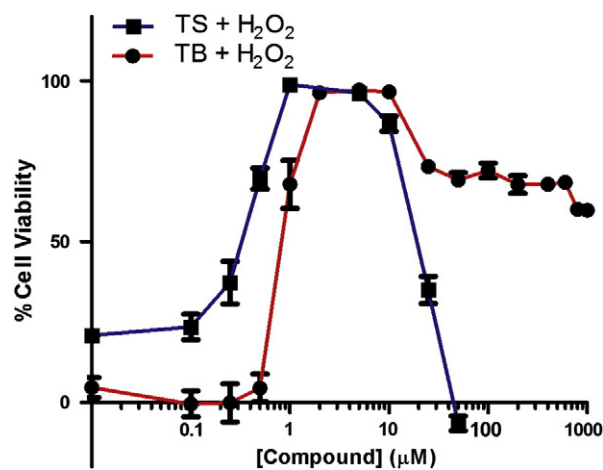


Fig. 11. The effect of TB and TS on ARPE-19 cells treated with a cytotoxic dose of $200 \mu\text{M}$ hydrogen peroxide. The chelator TS is protective within a narrow concentration window of $1\text{--}10 \mu\text{M}$, while the prochelator is protective at all concentrations tested over $1 \mu\text{M}$.

assessed in an in vitro assay. TB on the other hand, demonstrates several attributes that suggest it may be a useful prochelator for protection against oxidative damage in a biological context.

TB is stable in aqueous solutions, and a pH titration monitored by boron NMR reveals that under physiological conditions, the boronate exists as both the trigonal form and a solvent coordinated tetrahedral species. TB rapidly responds to hydrogen peroxide exposure by converting to the multidentate amine phenol chelator TS. The initial rates of oxidation of TB and TRENBSAM were compared under pseudo first-order conditions of hydrogen peroxide to reveal that TB oxidizes ten times faster than TRENBSAM ($k = 0.72 \text{ M}^{-1} \text{ s}^{-1}$ vs $0.07 \text{ M}^{-1} \text{ s}^{-1}$). This much faster rate may be beneficial for quick response of the prochelator to a toxic burst of hydrogen peroxide.

Both TS and TB are effective at preventing iron and copper-induced hydroxyl radical generation in an in vitro assay. Given the rate constant determined for TB oxidation, a $10 \mu\text{M}$ dose of prochelator would yield about $5 \mu\text{M}$ chelator after 30 min of exposure to $400 \mu\text{M}$ H_2O_2 and the conversion would be complete in about an hour. Because the Fenton reaction mixture in the in vitro assay shown in Fig. 9 was incubated for 60 min, the partial protection afforded by $10 \mu\text{M}$ TB is in agreement with the expected concentrations of generated chelator and the amount of iron in solution.

The effectiveness of TS at inhibiting the Fenton reaction likely derives from several factors. As shown by the crystal structure, one of these factors is the full coordination shell it provides to bind iron in a 6-coordinate octahedral site that prohibits direct access to an incoming reactant. Additionally, it has a significant affinity for iron. At pH 7.4, TS binds Fe(III) with an apparent $\log K'$ of 14.4, which corresponds to a dissociation constant (K_D) of 3.8 fM. For comparison, this affinity is slightly weaker than EDTA, which binds with a $\log K'$ of 15.9 at the same pH and is generally known as a strong chelating agent. Affinity is not the best indicator of inhibitors of metal-catalyzed oxidative stress, however. Iron complexes that catalyze hydroxyl radical formation are generally in coordination environments that support Fe(II)/Fe(III) redox cycling within a window of potentials between +460 mV and –160 mV vs. NHE [49]. This window is bound at one end by the $E_{1/2}$ of H_2O_2 at +460 mV, such that ferrous complexes with reduction potentials more positive than this value are not oxidized by H_2O_2 and therefore do not undergo Fenton chemistry. On the other end, complexes with reduction potentials more negative than –160 mV are stable as their ferric forms and are not reduced by superoxide, so do not redox-cycle by Haber-Weiss chemistry to generate hydroxyl radicals. With an $E_{1/2}$ of +120 mV vs. NHE, the FeEDTA complex falls within this window and is known to promote Fenton reactivity [1]. Here, the reduction potential of the FeTS complex at pH 7.4 was found to be –190 mV vs. NHE. While this $E_{1/2}$ is not as negative as that of many siderophores and siderophore-like models, which often have reduction potentials that range from –400 to –1000 mV vs. NHE, [50] it does fall outside of the ‘danger’ zone for Fenton chemistry.

In terms of metal ion preference, TS has very little affinity for Ca(II), as determined from a competition assay with the indicator fura-4F, suggesting that TS will not bind calcium in biological systems. It does, however, have appreciable affinity for divalent D-block metal ions, which is not surprising given the mixture of hard anionic oxygen and neutral nitrogen donors present in the ligand. The apparent affinities of TS for Zn(II) and Cu(II) were found to be $\log K' = 9.67$ and $\log K' = 15.87$, respectively. The ligand TS is therefore not inherently selective for Fe(III) over other metal ions; however, its masked prochelator version TB has negligible interactions with metal ions. The metal ion selectivity of TB/TS therefore does not derive from the coordination preferences of the chelator, but rather from the H_2O_2 responsiveness of the prochelator.

The toxicity profiles of TB and TS in cellular assays showed significant differences between the prochelator and chelator. Whereas the prochelator showed very little toxicity upon incubation with cells, TS showed 50% loss in viability at concentrations as low as $10 \mu\text{M}$

and complete cell death at higher concentrations. The cause of the dramatic toxicity is not currently known. However, when cells are dosed with TB or TS in conjunction with a toxic dose of hydrogen peroxide, it is clear that some protective effect is seen with both. Concentrations of TS as low as $1 \mu\text{M}$ rescue cells from peroxide-mediated death. However, this beneficial property has a very narrow window of efficacy, as concentrations above $10 \mu\text{M}$ fail to protect cells, likely due to the chelator's inherent toxicity in addition to the effects of the peroxide. In contrast to this narrow protective range for TS, TB shows a much broader window of protection. Concentrations as low as $2 \mu\text{M}$ of TB are completely protective. Given the rate constant of prochelator oxidation and the level of hydrogen peroxide, a $2 \mu\text{M}$ dose correlates to full conversion to the chelator in just under 2 h. In the case of high TB doses, the protective effect is still significant (~70% viability), though this indicates more cell toxicity than the presence of TB alone. A likely explanation is that over the same 2 h time period, enough TS could be produced to overshoot its protective capacity and induce its toxicity.

In conclusion, we have designed a new series of hexadentate prochelators to prevent iron and copper promoted oxidative stress. An important conclusion from this work is that masking the metal binding groups of TS in a hydrogen peroxide responsive manner increases the potential therapeutic window of this chelating agent.

Abbreviations

DFO	desferrioxamine
DMEM	Dulbecco's modified eagle medium
HEPES	4-(2-hydroxyethyl)-1-piperazineethanesulfonic acid
HRMS	high resolution mass spectrometry
HTS	protonated tris[2-hydroxybenzyl]2-aminoethyl]amine
LDH	lactate dehydrogenase
MEM	minimal essential medium
NHE	normal hydrogen electrode
PAR	(4-(2-pyridylazo)resorcinol)
PBS	phosphate buffered saline
ROS	reactive oxygen species
RPE	retinal pigment epithelial
TB	tris[(2-boronic acid-benzyl)2-aminoethyl]amine
TS	tris[2-hydroxybenzyl]2-aminoethyl]amine

Acknowledgements

We thank the US National Institutes of Health (Grants EY018922 and GM084176) for funding. KJF also acknowledges support from the Sloan Foundation and the Camille and Henry Dreyfus Foundation.

Appendix A. Supplementary material

Supplementary information. Supplementary data associated with this article, including UV/Vis spectra of metal competition reactions, cyclic voltammograms, and NMR spectra, can be found online. Full crystallographic data can be obtained free of charge from The Cambridge Crystallographic Data Centre (CCDC IDs: 817617–817619) at www.ccdc.cam.ac.uk/data_request/cif.

Supplementary data associated with this article can be found, in the online version, at [doi:10.1016/j.jinorgbio.2011.05.023](https://doi.org/10.1016/j.jinorgbio.2011.05.023).

References

- [1] M. Valko, H. Morris, M.T.D. Cronin, *Curr. Med. Chem.* 12 (2005) 1161–1208.
- [2] J.L. Dunaief, *Invest. Ophthalmol. Vis. Sci.* 47 (2006) 4660–4664.
- [3] D.W. Lee, J.K. Andersen, *J. Neurochem.* 112 (2010) 332–339.
- [4] D.B. Kell, *Arch. Toxicol.* 84 (2010) 825–889.
- [5] E. Gaggelli, H. Kozłowski, D. Valensin, G. Valensin, *Chem. Rev.* 106 (2006) 1995–2044.
- [6] K.J. Barnham, C.L. Masters, A.I. Bush, *Nat. Rev. Drug Discov.* 3 (2004) 205–214.

- [7] P. Zatta, D. Drago, S. Bolognin, S.L. Sensi, Trends Pharmacol. Sci. 30 (2009) 346–355.
- [8] L. Zecca, M.B.H. Youdim, P. Riederer, J.R. Conner, R.R. Crichton, Nat. Rev. Neurosci. 5 (2004) 863–873.
- [9] L.R. Perez, K.J. Franz, Dalton Trans. 39 (2010) 2177–2187.
- [10] R.R. Crichton, D.T. Dexter, R.J. Ward, Coord. Chem. Rev. 252 (2008) 1189–1199.
- [11] L.E. Scott, C. Orvig, Chem. Rev. 109 (2009) 4885–4910.
- [12] T.F. Tam, R. Leung-Toung, W. Li, Y. Wang, K. Karimian, M. Spino, Curr. Med. Chem. 10 (2003) 983–995.
- [13] G. Spyridon, A. Ioannis, C. Nikolaos, K. Aikaterini, T. Elana, P. Dimitrios, C. Aikaterini, A. Miltiadis, Open Ophthalmol. J. 4 (2010) 39–41.
- [14] A.H. Rahi, J.L. Hungerford, A.I. Ahmed, Br. J. Ophthalmol. 70 (1986) 373–381.
- [15] M. Sooriyaarachchi, J. Gailer, Dalton Trans. 39 (2010) 7466–7473.
- [16] L.K. Charkoudian, D.M. Pham, K.J. Franz, J. Am. Chem. Soc. 128 (2006) 12424–12425.
- [17] L.K. Charkoudian, D.M. Pham, A.M. Kwon, A.D. Vangeloff, K.J. Franz, Dalton Trans. (2007) 5031–5042.
- [18] L.K. Charkoudian, T. Dentchev, N. Lukinova, N. Wolkow, J.L. Dunaief, K.J. Franz, J. Inorg. Biochem. 102 (2008) 2130–2135.
- [19] M.G. Dickens, K.J. Franz, ChemBioChem 11 (2010) 59–62.
- [20] L.M. Hyman, C.J. Stephenson, M.G. Dickens, K.D. Shimizu, K.J. Franz, Dalton Trans. 39 (2010) 568–576.
- [21] T. Jirasomprasert, N.P. Morales, L.M.G. Limenta, S. Sirijaroonwong, P. Yamanont, P. Wilairat, S. Fucharoen, U. Chantharaksri, Free Radic. Res. 43 (2009) 485–491.
- [22] S.M. Cohen, M. Meyer, K.N. Raymond, J. Am. Chem. Soc. 120 (1998) 6277–6286.
- [23] D.F. Cook, D. Cummins, E.D. McKenzie, J. Chem. Soc., Dalton Trans. (1976) 1369–1375.
- [24] S. Liu, L. Gelmini, S.J. Rettig, R.C. Thompson, C. Orvig, J. Am. Chem. Soc. 114 (1992) 6081–6087.
- [25] P.K. Glasoe, F.A. Long, J. Phys. Chem. 64 (1960) 188–190.
- [26] B. Halliwell, J.M.C. Gutteridge, O.I. Aruoma, Anal. Biochem. 165 (1987) 215–219.
- [27] M. Hermes-Lima, P. Ponka, H.M. Schulman, Biochim. Biophys. Acta, Gen. Sub. 1523 (2000) 154–160.
- [28] D.T. Sawyer, A.J. Sobkowiak, J.R. Jr., Electrochemistry for Chemists, 2 ed. John Wiley & Sons, 1995.
- [29] A.E. Martell, R.M. Smith, NIST Standard Reference Database 46, 6.0, 2001.
- [30] H.M.D. Bandara, D.P. Kennedy, E. Akin, C.D. Incarvito, S.C. Burdette, Inorg. Chem. 48 (2009) 8445–8455.
- [31] L. Zhu, S.H. Shabbir, M. Gray, V.M. Lynch, S. Sorey, E.V. Anslyn, J. Am. Chem. Soc. 128 (2006) 1222–1232.
- [32] B.E. Collins, S. Sorey, A.E. Hargrove, S.H. Shabbir, V.M. Lynch, E.V. Anslyn, J. Org. Chem. 74 (2009) 4055–4060.
- [33] S.H. Shabbir, L.A. Joyce, G.M.da. Cruz, V.M. Lynch, S. Sorey, E.V. Anslyn, J. Am. Chem. Soc. 131 (2009) 13125–13131.
- [34] D.e. Hall, Boronic Acids: Preparation and Applications in Organic Synthesis and Medicine ed., Wiley-VCH Verlag GmbH & Co, Weinheim, 2005.
- [35] B. Wrackmeyer, Annu. Rep. NMR Spectrosc. 20 (1988) 61–203.
- [36] S. Hermanek, Chem. Rev. 92 (1992) 325–362.
- [37] L.A. Cabell, M.-K. Monahan, E.V. Anslyn, Tetrahedron Lett. 40 (1999) 7753–7756.
- [38] S.L. Wiskur, J.J. Lavigne, H. Ait-Haddou, V. Lynch, Y.H. Chiu, J.W. Canary, E.V. Anslyn, Org. Lett. 3 (2001) 1311–1314.
- [39] R.L. Giles, J.A.K. Howard, L.G.F. Patrick, M.R. Probert, G.E. Smith, A. Whiting, J. Organomet. Chem. 680 (2003) 257–262.
- [40] S.W. Coghlan, R.L. Giles, J.A.K. Howard, L.G.F. Patrick, M.R. Probert, G.E. Smith, A. Whiting, J. Organomet. Chem. 690 (2005) 4784–4793.
- [41] T.D. James, K.R.A.S. Sandanayake, R. Iguchi, S. Shinkai, J. Am. Chem. Soc. 117 (1995) 8982–8987.
- [42] G. Grynkiewicz, M. Poenie, R.Y. Tsien, J. Biol. Chem. 260 (1985) 3440–3450.
- [43] K.R. Gee, E.A. Archer, L.A. Lapham, M.E. Leonard, Z.-L. Zhou, J. Bingham, Z. Diwu, Bioorg. Med. Chem. Lett. 10 (2000) 1515–1518.
- [44] S. Liu, S.J. Rettig, C. Orvig, Inorg. Chem. 31 (1992) 5400–5407.
- [45] P. Bhattacharyya, J. Parr, A.M.Z. Slawin, Inorg. Chem. Commun. 2 (1999) 113–115.
- [46] A. Mustapha, J. Reglinski, A.R. Kennedy, Inorg. Chim. Acta 362 (2009) 1267–1274.
- [47] C.W. Conroy, P. Tyma, P.H. Daum, J.E. Erman, Biochim. Biophys. Acta 537 (1978) 62–69.
- [48] S. Steinhäuser, U. Heinz, M. Bartholoma, T. Weyhermüller, H. Nick, K. Hegetschweiler, Eur. J. Inorg. Chem. (2004) 4177–4192.
- [49] J.L. Pierre, M. Fontecave, Biometals 12 (1999) 195–199.
- [50] A.L. Crumbliss, J.M. Harrington, Adv. Inorg. Chem. 61 (2009) 179–250.